euspen's 23rd International Conference & Exhibition, Copenhagen, DK, June 2023
www.euspen.eu

Simulation and experimental study on material removal mechanism in milling of 70wt% Si/Al composite

Lianjia Xin[1], Guolong Zhao[1,*], Zhiwen Nian[1], Liang Li[1], Ning He[1]

[1]*College of Mechanical and Electrical Engineering, Nanjing University of Aeronautics and Astronautics, Nanjing 210016, P. R. China*

zhaogl@nuaa.edu.cn

Abstract
High-mass fraction silicon aluminium composite (Si/Al composite) is widely applied in a variety of fields, such as autommotive, radar, rail transit, space technology, due to its unique properties including excellent thermal conductivity, high stiffness, low density and good weldability. Surface quality and subsurface damages have significant influence on the service performance of Si/Al components. However, Si/Al composite is a difficult-to-machine material with machining characteristics of rapid tool wear and severe damages. In this paper, a constitutive model of 70wt% Si/Al composite was developed based on the Split Hopkinson Pressure Bar (SHPB) test, plate-impacts test and Si/Al interface cohesive zone model. A 3D cutting simulation model of Si/Al composite was established by python script and user subroutine in Abaqus, in which the characteristics of Si particles was taken into consideration. In addition, milling experiments were carried out to verify the simulation results. The material removal mechanisms were investigated, and it was found that the simulation results were in good agreement with the experimental results. Milling-induced damages including cracks, pits, matrix coatings, etc., were generated on the surface and subsurface due to the failure of reinforcement particles and the interaction between Si particles and Al matrix. Cutting speed had a significant influence on milling-induced damages. With the increase of cutting speed, the milling-induced damages were first alleviated and then worsened. Damage was barely observed on the surface machined with a cutting speed of 110 m/min and a feed rate of 0.02 mm per tooth. This study provides theoretical guidance for the suppression of milling-induced damage in Si/Al composite and other particle reinforced metal matrix composites.
Keywords: Si/Al composite; material removal mechanism; simulation; constitutive model; experimental verification;

1. Introduction

The demand for electronic packaging materials with high thermal conductivity and low thermal expansion coefficient has been on the rise in recent years. High-mass fraction silicon aluminium composite (Si/Al composite) is a relatively new electronic packaging material and a type of particle-reinforced metal matrix composite (PRMMC). Si/Al composite has a wide range of applications in industries such as automotive, rail transit, communication, and aerospace due to its superior thermal conductivity, low thermal expansion coefficient, good corrosion resistance, and wear resistance [1, 2]. The most common methods of machining Si/Al composite are mechanical machining processes, such as turning, milling, and drilling. However, the presence of hard Si particles in the composite makes mechanical machining a significant challenge, resulting in severe machining damage, rapid tool wear, and large machining vibration that limit its widespread use [3-5].

Visualizing the machining mechanism in the cutting process is challenging. The interaction between tool and workpiece in composite machining is highly complex and even more difficult to be characterized [6, 7]. Using finite element simulations is an effective and often-used approach for understanding the cutting mechanism. Niu et al. [8] developed a dynamic damage softening constitutive model for 50wt% Si/Al composite using the results of several mechanical experiments and conducted a verification test. The average absolute error of their constitutive model was only 4.93% and the dynamic compression behaviour of 50wt% Si/Al composite was defined effectively. However, it remains to be seen if the constitutive model is effective in describing the behavior of composites with higher silicon content. In addition, it should be noted that one constitutive model is not sufficient to simulate the material removal process. Using different constitutive models for different components of the material can provide a complete and more accurate description of the cutting process. Yu et al. [9] investigated the damage behaviour of PRMMCs using a two-dimension cutting simulation model. Reinforcement particles, matrix, and the interface between matrix and particle were defined, respectively. The relation between particle position and the cutting path was discussed to reveal the formation process of machining damage.

Due to the lack of one axis, two-dimensional models are only suitable for simulating orthogonal cutting. Fan et al. [10] developed a three-dimension cutting simulation model to investigate the material removal mechanism. The damage formation process was thoroughly discussed. However, the properties of the interface between the reinforcement and matrix were not defined. The reinforcement particles in the model were all idealized as cuboid structures of the same size, which resulted in an increase in simulation error.

In this work, a three-dimensional meso-simulation model for simulating the cutting of 70wt% Si/Al composite was established using image processing technology and statistical analysis. Experimental tests were conducted to validate the simulation model. The material removal mechanism of the composite was analysed. Additionally, this study investigated the effects of cutting speed on surface roughness. This work aims to provoke deeper thoughts on analysing the cutting mechanism of composite materials and provides guidance for reducing milling-induced damage in Si/Al composite and other PRMMCs.

2. Establishment of the simulation model

Due to a large amount of Si particles contained in 70wt% Si/Al composite, the material exhibits clear heterogeneity. To establish an accurate meso-simulation model, it is crucial to describe the heterogeneous characteristics of the composite. At the same time, it is also important to select an appropriate material constitutive model for the material. In the current work, an effective cutting model was developed by simulating the real cutting process considering both material structure and material properties. The process of establishing the simulation model for cutting 70wt% Si/Al composite is further explained in the next two sections.

2.1. Three-dimensional material model

The simulation accuracy can be improved by recreating the microstructure of the real material. Image processing technology is an effective approach to obtain the characteristics of Si particles. The procedure of image processing is shown in Fig. 1. OpenCV framework was used to analyse the morphologies image of 70wt% Si/Al composite under a scanning electron microscope (SEM), as shown in Fig. 1(a). The area and perimeter of single Si hard particle were obtained using filtering, morphological transformation, and image segmentation. The binarized image after the image processing is displayed in Fig. 1(b).

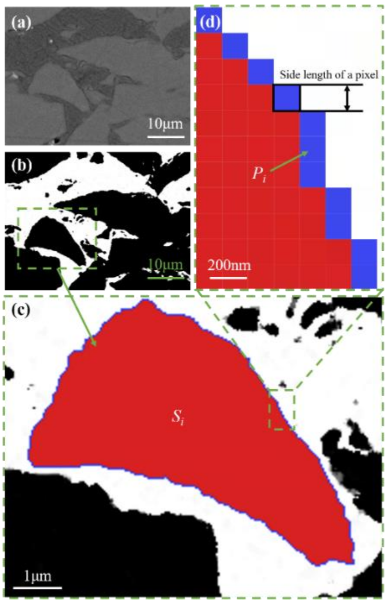

Figure 1. Image processing procedure. (a) the micro morphology of Si/Al composite, (b) binarization of the morphology image, (c) the area of a single particle and (d) the boundary of a single particle.

The area, S_i, and the perimeter, P_i, of a single particle, as illustrated in Fig. 1(c) and Fig. 1(d), can be given using Eq. (1) and Eq. (2). l_{pi} is set as the side length of a single pixel in SEM images.

$$S_i = l_{pi}^2 N_s \tag{1}$$

$$P_i = l_{pi} N_p \tag{2}$$

where N_s represents the number of pixels included in a single particle and N_p is the number of pixels on the particle boundary. The equivalent radius R_i of a single particle can be obtained as follows:

$$R_i = \frac{2S_i}{P_i} \tag{3}$$

assuming that the value of the equivalent radius, R_i, follows a Gaussian distribution. According to fitting analysis, the probability distribution function of R_i was obtained (Eq. (4)). The expectation $E(R_i)$ of the equivalent radius of Si particles is μ, and σ is the standard deviation of R_i.

$$f\left(R_i \middle| \mu, \sigma^2\right) = \frac{1}{\sqrt{2\pi}\sigma} \exp\left(-\frac{(R_i-\mu)^2}{2\sigma^2}\right) \tag{4}$$

Based on the Si content of 70wt% Si/Al composite, a python script was written to generate Si particles model via Abaqus secondary development interface. The three-dimensional composite model and structures of each part of the model are shown in Fig. 2.

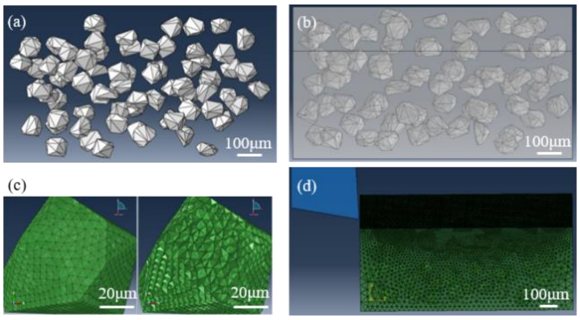

Figure 2. Establishment of material model: (a) Si particle model, (b) Al matrix model, (c) cohesive layer and (d) cutting simulation model.

2.2. Material constitutive model

During cutting, 70wt% Si/Al composite exhibits both ductile and brittle behavior. The highly brittle Si particles are destroyed under the action of cutting-edge. The high ductility Al matrix undergoes severe deformation, resulting in the generation of matrix coating damage. The Si/Al interface is debonded under the high cutting force, resulting in the formation of burrs. The three components of the composite exhibit three different behaviours. Therefore, the material properties of Si particles, Al matrix and Si/Al interface layer must be defined separately during the establishment of the cutting simulation model.

Johnson-Cook (JC) model is an often-used dynamic constitutive model for metal materials under large strain and high strain rate. Due to its simple form and the easy addition of correction items, JC constitutive model is widely applied to describe the dynamic behaviour of ductile materials. In this work, JC model was utilized to model the constitutive behaviour of Al matrix, and the expression is as follows.

$$\sigma = \left(A + B\varepsilon^n\right)\left[1 + C\ln\left(\frac{\dot{\varepsilon}}{\dot{\varepsilon}_0}\right)\right]\left[1 - \left(\frac{T - T_r}{T_m - T_r}\right)^m\right] \tag{5}$$

Where, σ is the equivalent stress, and ε is the equivalent plastic strain. The parameters A, B, and C are the initial yield stress, hardening modulus and strain rate strengthening coefficient, respectively. m, n, T_r, T, and T_m represent the material thermal softening index, strain hardening index, reference temperature, room temperature and material melting temperature. $\dot{\varepsilon}_0$ and $\dot{\varepsilon}$ are the reference strain rate and dimensionless strain rate, respectively. In addition, the initial damage of the Al matrix was also defined in the model.

The dynamic behaviour of Si particles was described using the Johnson-Holmquist II (JH2) constitutive, which was implemented in Abaqus using user subroutine. Based on the continuous damage theory, cracked Si particles were homogenized by the JH2 model and the damage behaviour was defined by reducing the strength of Si. JH2 constitutive model mainly includes three parts: a material continuous strength model, a damage model and a state equation. The model is defined by Eqs. (6)-(8).

$$\sigma^* = \sigma_i^* - D\left(\sigma_i^* - \sigma_f^*\right) \tag{6}$$

$$D = \sum \frac{\Delta\varepsilon_p}{\varepsilon_p^f} \tag{7}$$

$$P = K_1\mu_v + K_2\mu_v^{\ 2} + K_3\mu_v^{\ 3} \tag{8}$$

where, μ_v is the volume strain, σ^* is the dimensionless equivalent strength, D is the damage factor, σ_i^* represents the dimensionless equivalent strength of the completely undamaged material, σ_f* is the dimensionless equivalent strength of the completely damaged material, $\Delta\varepsilon_p$ is the cumulative integral of effective plastic strain during one cycle and ε^f_p is the ultimate plastic strain when the hydrostatic pressure is P. K_1, K_2 and K_3 are constants.

A cohesive zone model (CZM) was established to define the Si/Al interface of 70wt% Si/Al composite, as expressed in Eq. (9).

$$t=\begin{Bmatrix} t_n \\ t_s \\ t_t \end{Bmatrix}=\begin{bmatrix} M_{nn} & M_{ns} & M_{nt} \\ M_{ns} & M_{ss} & M_{st} \\ M_{nt} & M_{st} & M_{tt} \end{bmatrix}\begin{Bmatrix} \delta_n \\ \delta_s \\ \delta_t \end{Bmatrix}=K\delta \qquad (9)$$

where, subscript t and s are the shear directions, and subscript n is the normal direction. Parameters t, δ and M represents the stress, strain and modulus in different directions, respectively. The matrix in the above equation is the stiffness matrix of the Si/Al interface layer.

Finally, the tool was modelled as a rigid body to ensure the stability of the solution and convergence of the simulation.

3. Experimental verification

3.1. Workpiece material and milling tools

A 70wt% Si/Al composite block was first cut into small samples, and these samples were polished with abrasive paper on a standard polishing machine. The polished samples were cleaned in an ultrasonic cleaning machine with anhydrous ethanol as the medium for three minutes to clear any debris. Finally, samples with dimensions of 40 mm× 30 mm × 10 mm were selected as workpieces. The micro-morphology of the workpiece is shown in Fig. 1(a). The cutting tool used was a two-edged polycrystalline diamond flat-end mill with a diameter of 8 mm. The helix angle, radial rake angle, and radial clearance angle of the tool were 0°, 3°, and 5° respectively. The tool is shown in Fig. 3.

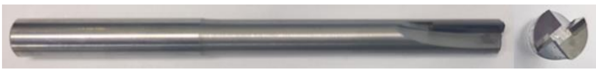

Figure 3. Milling tool used for experiments.

3.2. Experimental setup and design

To verify the cutting model of 70wt% Si/Al composite, side milling experiments under dry mode were conducted on a five-axis high-speed machining center (UPC710, Mikron, Switzerland). The schematic diagram of milling experiment configuration is shown in Fig. 4(b). During the experiments, the axial depth of cut, a_p, was set as 2 mm, the radial depth of cut, a_e, was set as 1mm, and the feed per tooth, f_z, was set as 0.02 mm. Multiple cutting speeds, v, were used in the study including 80 m/min, 90 m/min, 100 m/min, 110 m/min, and 120 m/min. The schematic diagram of the milling experiment configuration is shown in Fig. 4.

3.3. Characterizations

During the experiments, the cutting force was measured using a force measurement system, as shown in Fig. 4(a). The cutting force signal was first converted into an electric signal using a three-component piezoelectric dynamometer (9257B, Kistler, Switzerland). The electric signal was then transmitted to data acquisition card via charge amplifiers. The cutting force values were ultimately obtained using a processing software. The morphologies of the machined surface were examined using a scanning electron microscope (SEM, S4800, Hitachi, Japan) and an optical microscope (BX53M, Olympus, Japan). Additionally, the roughness of machined surface was measured using a three-dimensional profilometer (S Neox, Sensofar, Spain).

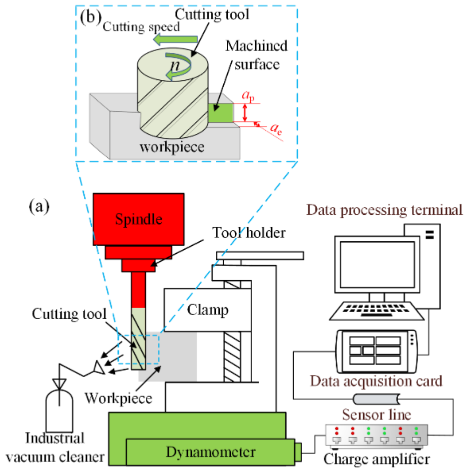

Figure 4. Schematic diagram of (a) milling experiment configuration and (b) down milling.

4. Results and discussions

4.1. Verification of cutting simulation model

The cutting simulation model can be verified by comparing the simulated cutting force with the experimentally measured cutting force. The comparison result is displayed in Fig. 5. The error bars of experimental results were the standard deviations of repeated measurements. The error bars of simulation results were the standard deviations of cutting force variation. With the increase in cutting speed, the cutting force of both results increases. The experimental cutting force increases from 45.3 N to 58.6 N. The maximum and minimum cutting force of simulation results are 41.1 N and 47.8 N, respectively. In the range of cutting speeds studied in the current, from 80 m/min to 120 m/min, the simulated cutting force is lower than the experimental results. The maximum and minimum errors of the simulated cutting force are 20% and 10%, respectively.

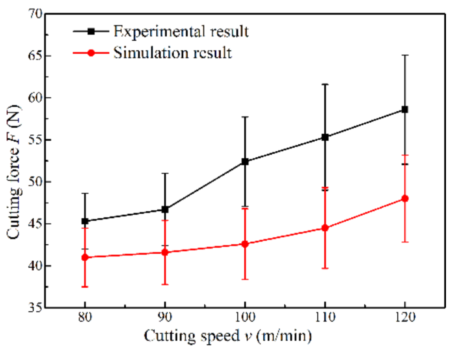

Figure 5. Comparison of simulation and experimental cutting force magnitude.

4.2. Material removal mechanism

The interaction between the tool and workpiece, as well as the material removal process can be described in detail by the simulation model. The ductile Al matrix undergoes deformation under the action of high hardness Si particles. The results of the simulation with the cutting speed set at 100 m/min is shown in Fig. 6.

At the initial stage of cutting, cutting-edge is in contact with the material surface (Fig. 6(a)). Cracks are generated on some of the Si particles on the material surface (Fig. 6(b)), while the other Si particles on the surface are squeezed into the material. At the same time, the Al matrix undergoes plastic deformation and the Si particles in the subsurface are subjected to the force of the Al matrix and surface Si particles. As the tool continues to move, the particles in contact with the cutting edge rotate and slip under the action of the cutting force. Debonding of particles occurs at the Si/Al interface, resulting in the formation of pits, as shown in Fig. 6(c) and Fig. 6(d). The plastic deformation of the Al matrix is aggravated. As the cutting process progresses (Fig. 6(e)), the Al matrix, along with some Si particles, slides out from the rake face, resulting in the formation of chips. Under the action of compressive stress, the Si particles in the subsurface are broken, resulting in the formation of cracks and pores in the composite (Fig. 6(f)). Additionally, the Al material on the flank face is smeared on the machined surface due to the large friction, causing the damage of matrix coating.

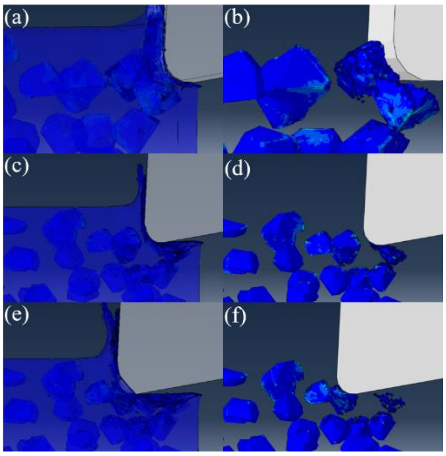

Figure 6. Cutting process simulation of (a), (b) cutting-in, (c), (d) forming chips and (e), (f) stable cutting stage with cutting speed of 100 m/min.

4.3. Surface quality

The surface roughness of experimental results at different cutting speeds is illustrated in Fig. 7. Each S_a value was averaged over 10 random areas measured on machined surface to avoid the occasionality. As the cutting speed increases from 80 m/min to 110 m/min, the surface roughness of the machined surface decreases. The micro morphologies of the machined surface under different cutting speed are illustrated in Fig. 8. At low cutting speeds, significant matrix coating and burr damages exist on the machined surface, as shown in Fig. 8(a) and Fig. 8(b).

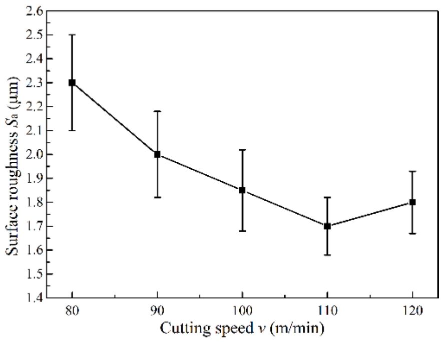

Figure 7. Roughness of machined surface under different cutting speeds.

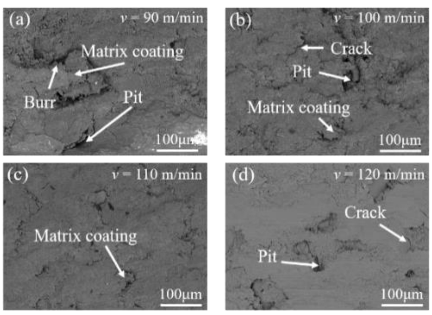

Figure 8. Micro morphologies of machined surface with cutting speed of (a) 90 m/min, (b) 100 m/min, (c) 110 m/min and (d) 120 m/min.

The damage of burr and matrix coating due to machining is reduced with the increase in cutting speed. Due to the higher speed, the cutting edge has more kinetic energy, the composite is removed more easily, and thus excessive plastic deformation of the Al matrix is avoided. When the cutting speed reaches 110 m/min, the surface roughness is minimum (S_a = 1.7 μm). In addition, SEM images show that damage is barely observed on the machined surface when the cutting speed is 110 m/min (Fig. 8(c)). With further increase in cutting speed, the surface roughness increases. This is due to the high brittleness reinforcement particles causing large machining vibration.

5. Conclusions

(1) The characterizations of Si particles were analysed based on image processing technology, and the microstructural model of 70wt% Si/Al composite was reconstructed in Abaqus. A constitutive model of the composite was established. As a result, a meso-simulation model was developed. The cutting force of simulation results with cutting speeds, *v*, from 80 m/min to 120 m/min were from 41.1 N to 47.8 N.

(2) Milling experiments were carried out to validate the simulation results. The simulation results were found to be in good agreement with experimental results, with a maximum error of 20% and a minimum error of 10%. The material removal mechanisms and the formation mechanism of machining damage were discussed. The interaction between reinforcement particles, matrix, and cutting-edge, resulted in the formation of machining damage such as matrix coating, cracks, burrs and pits on machined surface.

(3) An increase in cutting speed initially reduced the surface roughness but further increases led to an increase in roughness due to increased cutting vibration. The optimal cutting speed was found to be 110 m/min, for which the surface roughness, S_a, was minimum (1.7 μm).

References

[1] Wang J, Jiao X Y, Xie H L, Deng B and Xiong S M 2021 Crack configuration feature and fracture surface difference for high pressure Die casting hypereutectic Al-Si alloys in high cycle fatigue *Int. J. Fatigue.* **153** 106469

[2] Zhang L, Gan GS and Yang B 2011 Effect of *In-Situ* TiB_2 particles on the microstructure of spray-formed 70Si-Al alloy *Mater. Trans.* **52** 1646-9

[3] Wu Q, Xu W X and Zhang L C 2019 Microstructure-based modelling of fracture of particulate reinforced metal matrix composites *Compos. B. Eng.* **163** 384-92

[4] Kannan S and Kishawy H A 2006 Surface characteristics of machined aluminium metal matrix composites *Int. J. Mach. Tools. Manuf.* **46** 2017-25

[5] Liao Z R, Abdelhafeez A, Li H N, Yang Y, Gavalda Diaz O and Axinte D 2019 State-of-the-art of surface integrity in machining of metal matrix composites *Int. J. Mach. Tools. Manuf.* **143** 63-91

[6] Zhang L C, Wu Z H, Wu C H and Wu Q 2022 On the numerical modelling of composite machining *Compos. B. Eng.* **241** 110023

[7] Yang M H, Deng B, Huang Y, Peng F Y, Tang X W and Yan R 2023 Microstructural based constitutive modelling and subsurface microhardness prediction in machining of network-sturctured TiB_{2w}/TA15 composites *Compos. Sturct.* **305** 116470

[8] Niu Q L, Li S, Chen Y N, Li C P, Li S J, Ko T J, Li P N, Chen M and Qiu X Y 2022 A constitutive model of Al/50 wt%Si_p composites considering particle damage effects *J. Mater. Sci. Eng. A.* **836** 142762

[9] Yu W W, Chen J, Ming W W, An Q L and Chen M 2021 Experimental and FEM study of cutting mechanism and damage behavior of ceramic particles in orthogonal cutting SiC_p/Al composites *Ceram. Int.* **47** 7183-94

[10] Fan Y H, Xu Y S, Hao Z P and Lin J Q 2022 Dynamic behavior description and three-dimensional cutting simulation of SiC_p/Al composites with high volume fraction *J. Manuf. Process.* **77** 174-89